

DIFUSIÓN DE HIDRÓGENO EN HCP Zr HYDROGEN DIFFUSION IN HCP Zr

C. García¹ y V. P. Ramunni^{*2,3}

¹Instituto Sabato - UNSAM/CNEA, Av. Gral. Paz 1499, (1650) San Martín - Argentina.

²CONICET Godoy Cruz 2390 (C1425FQD) - Argentina.

³Gcia. Materiales-CNEA, Av. Gral. Paz 1499, (1650) San Martín - Argentina.

Recibido: 02/06/2021 ; Aceptado: 27/07/2021

Estudiamos el comportamiento del hidrógeno (H) en las fases puras α , β Zr y β Nb, empleando los códigos de primeros principios Siesta y Vasp, basados en la teoría del funcional de la densidad (DFT). Calculamos la energía de solución del hidrógeno, la energía de unión de los complejos H-H y H-Nb, como también la energía de mezcla del sistema Zr-Nb. Además, propusimos un modelo simple para el estudio de la difusión del H (D_H) mediado por un mecanismo intersticial en la fase hcp del Zr. Encontramos que el hidrógeno intersticial difunde isotrópicamente según $D_H = 1.1 \times 10^{-7} \exp(-42 \text{ KJ.mol}^{-1}/RT)$ (m^2/s). Nuestros resultados están en buen acuerdo con los datos experimentales y otras técnicas numéricas de Montecarlo cinético (KMC). Calculamos también, las energías de formación de los tres hidruros más estables en la fase hcp Zr.

Palabras clave: Hidrógeno, Difusión, Hidruros de circonio, α Zr, cálculos ab-initio.

We study the behavior of hydrogen (H) in the α and β phases of Zr and in the β phase of Nb, using the Siesta and Vasp first principles codes based on the density functional theory (DFT). We calculate the hydrogen solution energy, the binding energy of the H-H and H-Nb complexes, as well as, the mixing energy of the Zr-Nb system. Furthermore, we have proposed a simple model for the study of the hydrogen diffusion (D_H) mediated by interstitial mechanism in hcp Zr. We find that interstitial hydrogen diffuses isotropically according to $D_H = 1.1 \times 10^{-7} \exp(-42 \text{ KJ.mol}^{-1}/RT)$ (m^2/s). Our results are in good agreement with experimental data and other Kinetic Monte Carlo (KMC) calculations. Finally, the formation energies of the three most stable hydrides in the hcp Zr phase were also calculated.

Keywords: Hydrogen, Diffusion, Zirconium-Hydrides, Zr-Nb, ab-initio calculations.

<https://doi.org/10.31527/analesafa.2021.32.4.120>



ISSN 1850-1168 (online)

I. INTRODUCCIÓN

In the context of the Hydride Delayed Cracking phenomena (DHC), Zirconium based alloys are currently used in reactors due to their low neutron absorption and their good response to high temperature corrosion. Since hydrogen can be present in the alloys as a remnant impurity of the manufacturing process, and can also enter during the service life of the material, it is very important to evaluate the response of the alloys to hydrogen.

The microstructure, solubility and diffusion coefficient of H in the alloy are variables that allow us understand the DHC phenomena. For example, the Zr-2.5Nb alloy is bi-phasic with grains of phase α (hcp, with 0.6% Nb) surrounded by plates of β Zr phase (bcc, with 20% Nb).

With thermal treatments, the original plates of β Zr lose their continuity and interrupts the fast paths for the hydrogen diffusion in the axial direction of the tube and, at the same time, their percentage of Nb is altered evolving to the stable phase β Nb (bcc, with 90 - 100%Nb).

From this experimental evidence, the following questions arise:

1. Since β Nb must have a hydrogen solubility lower than that of pure Nb, then: It is possible to calculate the

solubility of H in pure Nb and of the Zr-Nb alloys, with different percentages of Nb?

2. Is the loss of continuity of the original sheets effectively responsible for the observed decrease in the diffusion coefficient of H as time passes at a given temperature?
3. Is the diffusion and / or solubility of hydrogen in the alloy affected by the Nb content?

This is a work prior to that carried out in Ref. [1], in which the authors have successfully answered questions 2 and 3 posed by our experiments. Here we focused on the study of the hydrogen's diffusivity on α Zr.

Concerning atomic diffusion, several efficient methods have been developed in recent years for finding activated states or, mathematically, saddle points from which diffusion can be studied. Here we employ the Monomer one, developed previously in our laboratory [2] and The Dimer method [3] as implemented in Vasp [4]. The Monomer, in coupled to Siesta's code [5] to be interfaced as a subroutine [6].

The Monomer computes the least local curvature of the potential energy surface using only the forces furnished by Siesta. The force component along the corresponding eigenvector is then reversed (pointing 'up hill'), thus defining

* vpram@cnea.gov.ar

a pseudo force that drives the system towards saddles. Both, local curvature and configuration displacement stages are performed within independent conjugate gradients loops. The method is akin to the Dimer one from the literature [3], but roughly employs half the number of force evaluations.

These methods are very efficient at obtaining the migration barriers from which we study the atomic diffusion in metals. In this way, Ishioka and Koiwa [7] have studied the interstitial diffusion in hcp metals, involving octahedral and tetrahedral sites. They have proposed an on-lattice random walk model to derive the diffusivities of impurity atoms on a crystal lattice containing multiple sublattices, such as the octahedral and tetrahedral sites in hcp crystals.

Here we focused on the study of the hydrogen's behavior in Zr-Nb. In this sense we study some relevant diffusion parameters, namely: (i) the hydrogen solubility, (ii) the hydrogen binding energies of the H-H and H-Nb complexes, (iii) the mixing solution energy of Nb-Zr and (iv) the hydrogen diffusion coefficients in hcp Zr. With this purpose, we perform ab-initio calculations with Siesta [5] and Vasp [4], in order to obtain the hydrogen migration barriers in the bulk of α Zr using the model developed in Ref. [7]. Classical calculations were also performed in order to check some structure consistence.

The present paper is structured as follows: Section II describes our calculation methodology with the DFT based codes as Siesta and Vasp, and from classical codes. Sections III show the way as the lattice parameter is calculated from the fit of a third-order Birch-Murnagahn equation of state, EOS, [8]. Section IV, is devoted to summarize the energetic of Hydrogen in the Zr-Nb system. Section V describes the way as the H-diffusion coefficients were calculated in α Zr together with our numerical results. In brief, Section VI, describes the structure of the three stable zirconium-hydrides in α Zr. The last section presents some conclusions.

II. CALCULATION METHODOLOGY

Ab initio calculations were performed as implemented in Siesta and Vasp. Siesta, is a freely available code [5], which is based on pseudopotentials and numerical, atomic-like, basis functions. The pseudopotential and basis for Zr are according to Ref. [6]. Pseudopotential for H was downloaded from Siesta's home page, and the corresponding base was automatically generated using the code itself.

Present Siesta calculations were carried out within the generalized gradient approximation (GGA) for exchange and correlation, according to the PBE parameterization described in Ref. [9]. A spatial mesh cutoff of 460.0 Ry were used, with a smearing temperature of 0.15 eV, within a Fermi-Dirac scheme. Reciprocal space is partitioned in a $5 \times 5 \times 5$ Monkhorst-Pack grid. All calculations were atomically relaxed, though the cell boundary remains fixed. For hydrogen, we used a so called TZDP basis with a split norm parameter of 0.5, which is the accurate one that most efficiently relaxes the bulk containing H.

Vasp uses a projector augmented-wave formalism to describe the interactions between atoms [10]. An energy cutoff of 460 eV and fine Γ -centered k-point meshes automatically generated with the Monkhorst-Pack scheme [11] of

$5 \times 5 \times 5$ -k points mesh ensured electronic convergence of the calculations. For the term of exchange and correlation we use the PBE-GGA approximation, with the Methfessel-Paxton broadening scheme with a 0.3 eV width. Concerning optimum structures, relaxation was done until the residual forces were below 0.02 eV/Å.

In both, Siesta and Vasp, we have used two supercell sizes of 48 and 54 atoms, respectively for α Zr and β Nb. The supercell of α Zr with 48 atoms is constructed by reproducing the conventional cell, of 4 atoms, along the lattice vectors of the hexagonal primitive cell a, b and c, in $2 \times 3 \times 2$.

In addition, we have performed calculations with the molecular statics technique (MS), implemented in an in-house code, provided with suitable EAM interatomic potentials for Zr [12]. We use a simulation cell of $15 \times 10 \times 10$ and $20 \times 20 \times 20$ respectively containing 6000 Zr or Nb atoms, with periodic boundary conditions.

These methods are very efficient at obtaining the equilibrium positions of the atoms by relaxing the structure via the conjugate gradients technique. Impurity and defect relaxation, includes interstitial H atoms in α Zr, β Nb, as well as, in the Zr-Nb alloy structure. The needed migration barriers of several jumps were calculated coupling both EAM and Siesta techniques to the Monomer method [2, 6], while we used the DIMER as implemented in Vasp [3].

Finally, our calculations were carried out at constant volume, and therefore the enthalpic barrier $\Delta H = \Delta U + p\Delta V$ is equal to the internal energy barrier ΔU .

The empirical formula (EF)

The EF is an expression that represents the simplest proportion in which the atoms are present in the alloy. In the case of the Zr-2.5Nb alloy, we start from a hypothetical sample with 100 gr of Zr-2.5Nb. From the % of Nb we defined that in 100 gr of the sample there are 2.5 gr of Nb while the rest, $(100-2.5) = 97.5$ gr, are of Zr. The moles of Zr and Nb that are present in those 100 gr of Zr-2.5Nb, are obtained through the ratio between the grams of each species in the sample by their respective molecular weights, $P_M^{Zr} = 91.224$ and $P_M^{Nb} = 92.90637$, as,

$$97.5 \text{ gr Zr} / 91.224 = 1.0057 \text{ moles of Zr,} \quad (1)$$

$$2.5 \text{ gr Nb} / 92.90637 = 0.0269 \text{ moles of Nb.} \quad (2)$$

In Eqs. (1) and (2) the ratio between species that contains the least number of moles gives the empirical formula $Zr_{37} : Nb_1$ for the alloy. This assumes that Nb atoms are located at periodic positions and not randomly; Also, this does not consider the different compositions of the alpha and beta phases.

From this result, we were considered two sizes of supercells, one of 36 atoms of Zr and another one with 48 atoms of Zr.

III. STRUCTURE OPTIMIZATION

For β Nb and β Zr, in order to better describe bulk zirconium properties, we determine a cut-off for the needed size of k-point mesh. On a $1 \times 1 \times 1$ cell consisting of two Nb or Zr atoms, several calculations were done using k-point meshes with sizes of $12 \times 12 \times 8$, $16 \times 16 \times 10$, $20 \times 20 \times 14$,

24 × 24 × 16, 28 × 28 × 18 and 32 × 32 × 20 with the use of 95, 180, 352, 549, 800 and 1122 irreducible k-points, respectively.

Using a general convergence cut-off of 5 meV/atom, it was shown that the choice of 20 × 20 × 14 k-point mesh would be sufficient to represent the both, Nb and Zr 1 × 1 × 1 supercells while keeping the computational effort at the minimum level. In subsequent calculations, choice of k-point mesh would be made based on the ratio between the size of the new supercell and that of the 1 × 1 × 1 supercell.

With the chosen k-point mesh, equation of state calculations were done in determining the computational lattice parameters of bulk βZr and βNb as follows: We perform an automated volume scan by means of a shell script loop.sh, with lattice parameters above and below the experimental value. Then, the procedure was to get the energy as a function of volume using by regression fitting DFT results to third-order Birch-Murnagahn equation of state, EOS, [8].

$$E(V) = E_0 + \frac{9V_0B_0}{16} \left\{ \left[\left(\frac{V_0}{V} \right)^{2/3} - 1 \right]^3 B'_0 + \left[\left(\frac{V_0}{V} \right)^{2/3} - 1 \right]^2 \left[6 - 4 \left(\frac{V_0}{V} \right)^{2/3} \right] \right\} \quad (3)$$

In Eq. (3), V_0 was found from the regression fitting in Fig. 1, which corresponds to the cell volume that result in the lowest possible total energy of the system. One last calculation to calculate the Zr lattice parameter was to optimize the ionic structure of a zirconium cell with a fixed volume equal to the value of V_0 . In addition, by getting the energy as a function of volume using third-order Birch-Murnagahn EOS, information about bulk modulus was also found.

The optimization procedure is also used with hcp structures. The fitting of the best a and c or c/a for hcp crystals is more difficult than in the previous case of the cubic lattices. This is because for hcp alloys, one should define a global minimum of the total energy of a crystal as a function of both, the volume of the unit cell and the structural relation c/a .

We have obtained a lattice parameter of $a_{Nb} = 3.304 \text{ \AA}$ and $a_{Nb} = 3.301 \text{ \AA}$ for a supercell containing 16 and 54 Nb atoms, respectively.

Also, the above procedure, is performed in order to obtain the optimal lattice parameter of the structure including interstitial (H) and substitutional (Nb) defects. For αZr and αZr containing impurities, a test value of structural relation c/a was fixed. The standard optimization procedure, like in the case of cubic lattices, was used to define the optimal volume of the unit cell corresponding to the minimum of the total energy as a function of the unit cell volume, $E_{min}^{(i)}(c/a)_i$, where $i=1, \dots, N$, the number of test values for the structural relation c/a .

The obtained empiric data as the dependence $E_{min}(c/a)$, were approximated by the functional dependence. The minimum of this dependence corresponds to the optimal value of the structural relation $(c/a)_{opt}$. Next, for the determined $(c/a)_{opt}$, the standard optimization procedure was made to determine a global minimum of the total energy and the op-

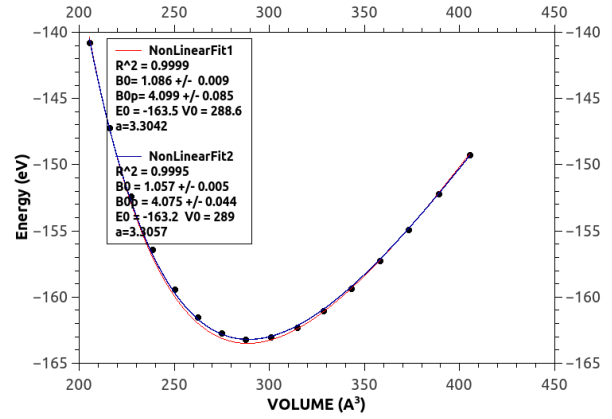


FIG. 1: Optimized lattice parameter of a βNb supercell containing 16 atoms.

timal unit cell volume, respectively.

Using the standard definition for the volume of the HCP unit cell $V_{hcp} = (c/a)_{opt} a_{hcp}^3 \sin(\frac{2\pi}{3})$ the optimal lattice constant a_{hcp} was determined for each case. Table 1, summarizes present results of the optimized lattice parameters from Zr and Nb.

Table 1 reports the calculated lattice parameters of α, β Zr and β Nb, namely: The lattice parameters, a and c/a , the Bulk modulus, B , the Cohsive energy, E_c , the vacancy formation energy, E_f^v , and the vacancy migration energy, E_m^v , in comparison with experimental and theoretical values reported in the literature.

Fig. 1, show our results of the optimized lattice parameter from the fit of Eq. (3) of a supercell containing 16 atoms of βNb. In this case the Bulk modulus was obtained, as well as, the resulting pressure of the supercell after relaxation. The same procedure was followed from 2 up to 54 atoms of Nb and Zr atoms with bcc structure.

TABLE 1: Lattice parameter (in Å) and the vacancy formation and migration energy (in eV).

αZr	Vasp/Siesta N=48	Vasp N=36	Vasp Ref. [13]	EAM N=6000	Exp.
a	3.237/3.239	3.240	3.237	3.2171	3.232 [14]
c	5.176/5.185	5.186	5.183	-	5.141 [15]
c/a	1.599/1.601	1.601	1.601	1.6046	1.5929 [14]
E_f^v	1.89/1.96	2.202	-	1.79	1.750 [15]
E_c	6.25	6.28	6.34	6.25	6.25 [16]
E_f^v	1.79	2.00	2.02	-	1.74 [16]
E_m^v in (c) (eV)	0.61	0.61	-	0.61	0.60 [17]
E_m^v in (a) (eV)	0.66	0.65	-	0.66	0.62 [18]
βNb	Vasp/Siesta N=108	Vasp N=54	Vasp Ref. [19]	EAM Ref. [20]	Exp.
a (Å)	3.303/3.308	3.304	3.309	3.3000	3.303 [21]
E_f^v	2.680/2.704	2.72	2.700	-	-
E_c	7.610/7.730	7.64	-	7.57	7.57 [16]
E_f^v	2.76	2.81	2.88 [22]	2.75	2.75 [23]
E_m^v	0.65	0.70	0.55 [24]	0.67	-

The comparison in Table 1 shows that the predicted geometries of the GGA (PBE) slightly overestimated the experimental lattice parameters. Although the regression fitting of the EOS in Eq. (3) overestimates V_0 by about 1.0%, this discrepancy between the DFT results and the reported experimental data was acceptable for this study. Then, the current set up of zirconium supercells with the chosen k-points mesh is approximately accurate in representing the actual zirconium and niobium metal structure.

The dependence of the lattice parameter, a_{Zr} , for β Zr-Nb alloys versus niobium concentration was previously evaluated in Ref. [25]. The authors have shown that with an increase in the niobium concentration the lattice constant decreases according to the linear law. This result is consistent with the well known approximate empirical rule, called in metallurgy Vegard's law. Also, at 0% of Nb the lattice parameter of β Zr is $a_{Zr}^{bcc} = 3.5634 \text{ \AA}$ while for pure β Nb is $a_{Nb}^{bcc} = 3.3004 \text{ \AA}$. Present calculations give $a_{Zr}^{bcc} = 3.5629 \text{ \AA}$.

IV. THE ENERGETIC OF THE Zr-Nb SYSTEM

IV.1 Mixing solution energy

The mixing solution energy, $\Omega_{mix}^{\alpha,\beta}$, of a substitutional B atom in a matrix of A atoms with α or β structure, is obtained as [19],

$$\Delta E[A_{N-M}B_M] = E[A_{N-M}B_M] - (N-M)E_0^A[A] - \frac{M}{N}E_0^B[B], \quad (4)$$

with $E[A_{N-M}B_M]$ the energy of the supercell with (N-M) A atoms and M B-atoms, $E_0^A[A]$ the reference energy of the matrix calculated with the same supercell and $E_0^B[B]$ the energy per atom of B in its state of reference (bcc for β Nb and hcp for α Zr). This excess energy is the solution energy weighted by the solute concentration $\chi_B = \frac{M}{N}$ as in Ref. [19],

$$\Delta E[A_{N-M}B_M] = \chi_B \Omega_{mix}^{\alpha,\beta}, \quad (5)$$

High and positive values of Eq. (5), show a strong tendency to Zr and Nb atoms not to mix in the Zr-Nb alloy. Here, for the diluted limit, we have used a supercell of 108 and 144 atoms respectively for bcc Nb and hcp Zr.

As $\chi_B = \frac{M}{N}$ and defining $x = \chi_{Zr} = 1 - \chi_{Nb}$ we obtain $\Omega^{\beta Nb}(x \rightarrow 0) = 0.322 \text{ eV}$ for a substitutional Zr diluted in β Nb, and $\Omega^{\alpha Zr}(x \rightarrow 0) = 0.632 \text{ eV}$ for a substitutional Nb atom in α Zr. The last results are in agreement with previous DFT ones of 0.61 eV [26] and 0.68 eV [27].

Our results show that Nb has a low solubility in α Zr given the high value of 0.63 eV, while Zr has high solubility in β Nb. For the supercells with 54 and 48 atoms of β Nb and α Zr, $\Omega^{\beta Nb}(x \rightarrow 0) = 0.34 \text{ eV}$ and $\Omega^{\alpha Zr}(x \rightarrow 0) = 0.641 \text{ eV}$, respectively.

IV.2 Hydrogen solution energies in α Zr and β Nb

The hydrogen solution energy, E_S , at stable sites were calculated according to the following expression [28],

$$E_S^H = E(N, H) - E(N) - \frac{1}{2}E(H_2) - E_{ZPE}. \quad (6)$$

In Eq. (6) $E(N, H)$ is the energy of the supercell containing N atoms plus an absorbed hydrogen at a determined interstitial site, $E(N)$ the energy of supercell without defects, $\frac{1}{2}E(H_2)$ the energy of the hydrogen in the gaseous phase, and E_{ZPE} , the zero point energy (ZPE) that corresponds to quantum corrections. The value of the solution energy in a given site gives us information about the stability of such a site.

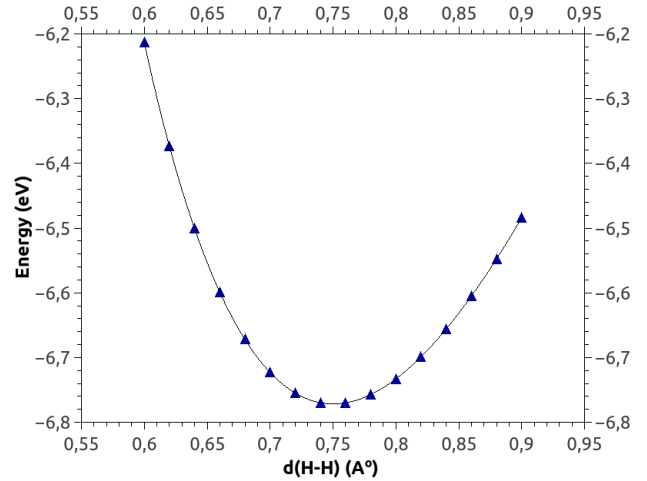


FIG. 2: The fitted hydrogen molecule, H_2 , bond length.

In Eq. (6), the third term corresponds to half of the total energy of the hydrogen molecule, is calculated using a cell of sides $10 \times 10 \times 10 \text{ \AA}^3$ containing only the dimer, H_2 , in the center of the cell for a single k-point. While the last term, correspond to the zero point energy due to quantum corrections.

Fig. 2 shows the obtained equilibrium bond length of 0.750 Å for the hydrogen molecule, and a dimer energy of 6.765 eV, from which we calculate a binding energy of 4.54 eV for the hydrogen molecule, in agreement with experimental values of 0.741 Å, and 4.75 eV [29], respectively.

The calculated H_2 vibration frequency are 4401 cm^{-1} , that agrees with the experimental value of 4395 cm^{-1} [30]. Finally, present result of the ZPE 0.27 eV, reproduces the experimental value 0.274 eV [29]. Table 2, summarizes our results of the H solution energy in the α Zr and β Nb respectively for a supercell of 48 and 54 atoms. High and negative

TABLE 2: Hydrogen solution energy, E_S^H (in eV) calculated with *Siesta/Vasp*.

System	E_S^H	H-Site	Refs.
α Zr ₄₈ H	-0.481	T	-0.609 [30]
α Zr ₄₈ H	-0.407	O	-0.549 [30]
β Nb ₅₄ H	-0.323	T	-0.340 [31]
β Nb ₅₄ H	-0.052	O	-0.030 [31]
α Zr ₄₈ H ₂	-0.963	T	-
α Zr ₄₈ H ₂	-0.637	O	-

values of the solution energies mean stable sites, while positive values can infer that the site will be unoccupied or, the site is not favorable for hydrogen solubilization.

The results in Table 2 reveal that H is highly soluble on both the T and O sites of α Zr phase, with the following energy relationship $E_S^H(T) > E_S^H(O)$. Concerning β Nb, H preferentially dissolves at the T site, whose solubility is much higher than at the O site. In regarding the energy of solution for the 2H in the α Zr phase, we observe that the T site is the preferential site for 2H whose energy of solution is more than double that of the isolated H in the same phase, showing that there is a slight interaction between the 2H.

IV.3 Binding energies

The hydrogen binding energy in a crystal containing N atoms of Zr plus k atoms of Nb on substitutional sites, was calculated with the following expression,

$$E_b = \{E(Zr_{N-k}Nb_kH_n) + (n+k-1) \times E(Zr_N)\} - \{k \times E(Zr_{N-1}Nb_1) + n \times E(Zr_NH_1)\}. \quad (7)$$

In Eq. (7) $E(Zr_{N-k}Nb_kH_n)$ and $E(Zr_{N-1}Nb_1)$ are respectively the energy of the supercell of Zr containing k substitutional atom of Nb, plus n -atoms of interstitial H, and the energy of the supercell with $(N-1)$ atoms of Zr plus a substitutional Nb. $E(Zr_NH_1)$ is the energy of the crystal containing N -atoms of Zr with a single interstitial H at its minimum configuration, while $E(Zr_N)$ is the energy of the perfect Zr lattice. Negative/positive values of E_b indicate repulsion/attraction between the H and the solute atom. Table 3 summarizes present results with Siesta and Vasp.

TABLE 3: Binding energies (in eV) with Siesta/Vasp calculations for a supercell with $N=48$ atoms of Zr, $n=1$ or 2 H atoms and $k=1$ atom of substitutional Nb. T_a and T_c correspond to tetrahedral sites for H in the basal and axial axes, respectively.

αZr	$E_b^{T_c}$	$E_b^{T_a}$	E_b^O
H-H	0.47/0.31	0.01/-0.02	0.12/0.12
Nb-H	0.11/0.29	0.08/0.06	0.05/0.04
Nb-2H	-0.01/-0.02	0.31/0.44	0.01/-0.02

Our calculations predict T-sites as the preferential sites of hydrogen dissolved in αZr , with $E_T - E_O = 0.06$ eV the energy difference between T- and O- hydrogen sites. In presence of Nb, this energy difference was maintained.

Results in Table 3, show that E_b were mostly positive, indicating that the interactions are attractive, that is, energetically favorable for the formation of the complexes, according to Domain et al. [32].

The exception is the binding energy of -0.01 / -0.02 eV, weak and negative, showing that the two T- hydrogen do not interact with Nb in the axial plane. The other negative energy of -0.02 eV reveal a slight repulsion between the two O-hydrogen first neighbors of Nb, in the basal plane.

From values in Table 3, we assume that the presence of Nb in αZr , with a positive binding energy with H, can be interpreted as a reduction in the hydrogen diffusivity by the hydrogen trapped locally by the Nb atom.

V. HYDROGEN DIFFUSION COEFFICIENT

Hydrogen diffusion in hcp Zr involving T and O sites driven by interstitial mechanism were studied with a model proposed by Ishioka and Koiwa [33], using an on-lattice random walk model for hcp crystals. The diffusivity along $\langle c \rangle$ and $\langle a \rangle$ directions are expressed as,

$$D_c = \frac{\omega_{TO}(3\omega_{OO}\omega_{TO} + 2\omega_{OO}\omega_{TT} + 3\omega_{TT}\omega_{OT})}{4(2\omega_{TT} + 3\omega_{TO})(\omega_{TO} + 2\omega_{OT})} c^2, \quad (8)$$

$$D_a = \frac{\omega_{TO}\omega_{OT}}{\omega_{TO} + 2\omega_{OT}} a^2. \quad (9)$$

In Eqs. (8) and (9), ω_{ij} are the mean jump frequencies ω of the four possible hydrogen transitions, namely: $T \rightarrow T$, $O \rightarrow O$, $T \rightarrow O$ and $O \rightarrow T$.

In order to compute the mean jump frequencies ω_α in Eqs. (8) and (9), we use the Vineyard formalism [34], that corresponds to the classical limit, where the vibrational prefactors, v_0^* , do not depend on the temperature, that is

$$\omega_\alpha = v_\alpha^* \exp(-E_\alpha^m/k_B T). \quad (10)$$

In (10), E_α^m are the vacancy migration energies at $T = 0$ K, while

$$v_\alpha^* = \left(\prod_{i=1}^{3N-3} v_i^I \right)_\alpha / \left(\prod_{i=1}^{3N-4} v_i^S \right)_\alpha = v_0 \exp\left(\frac{S_\alpha^m}{k_B}\right), \quad (11)$$

with v_i^I and v_i^S the frequencies of the normal vibrational modes at the initial and saddle points, respectively, and v_0 the Deby's frequency. Migration barriers were calculated with the Monomer [2] coupled to Siesta [6], and the DIMER Method [3] as implemented in Vasp. Present results of the migration barriers (in eV) are summarized in Table 4.

TABLE 4: Hydrogen migration energies, E_m (in eV), in αZr calculated with Siesta and Vasp for a supercell of $N=48$ atoms of Zr and one interstitial H.

Jump	Siesta	Vasp	Ref. [7]
T-T	0.14	0.12	0.129
T-O	0.45	0.39	0.406
T-T	0.36	0.32	0.346
O-O	0.42	0.37	0.398

The anisotropy of hydrogen diffusion in αZr has been widely studied from Monte Carlo Kinetic (KMC) [7, 35], using individual H jumps between first neighbors (1NN) T and O sites. These authors have found an expression of the diffusion coefficient $D_H = 5.55 \times 10^{-7} \exp(0.41 \text{ eV}/RT) \text{ m}^2 \text{ s}^{-1}$, which is higher than the experimental value of $D_H = (6.84 - 7.82) \times 10^{-7} \exp([0.46 - 0.47] \text{ eV}/RT) \text{ m}^2 \text{ s}^{-1}$ [36] for $T < 1000$ K.

On the other hand, Sawatzky et al. [35] have obtained the diffusion coefficient for hydrogen in annealed and extruded specimens as $D_H = 1.17 \times 10^{-7} \text{ m}^2 \text{ s}^{-1}$ with $Q_D = 33.60$ KJ/mol over the temperature range 473 to 973 K from KMC calculations. While, Zhang et al. [7], are who have obtained results closer to the experimental ones. Fig. 3 shows our results of D_c and D_a in αZr calculated from Eqs. (8) and (9) using both, Siesta and Vasp codes.

Experimental data from Ref. [37] and previous numerical results from KMC calculations in Ref. [35], are also included. Experimental results of hydrogen diffusion in αZr -2.5Nb [38], are shown in blue line.

The mean jump frequencies were calculated from Eqs. (10) and (11) with the migration barriers listed in Table 4, verify $\omega_1 > \omega_3 > \omega_4 > \omega_2$.

Fig. 3(c) shows the behavior of the mean jump frequencies with the inverse of the temperature.

Fig. 3(a)-(c), show our numerical results of D_H and the mean jump frequencies in αZr in terms of $1/T$ (in K^{-1}),

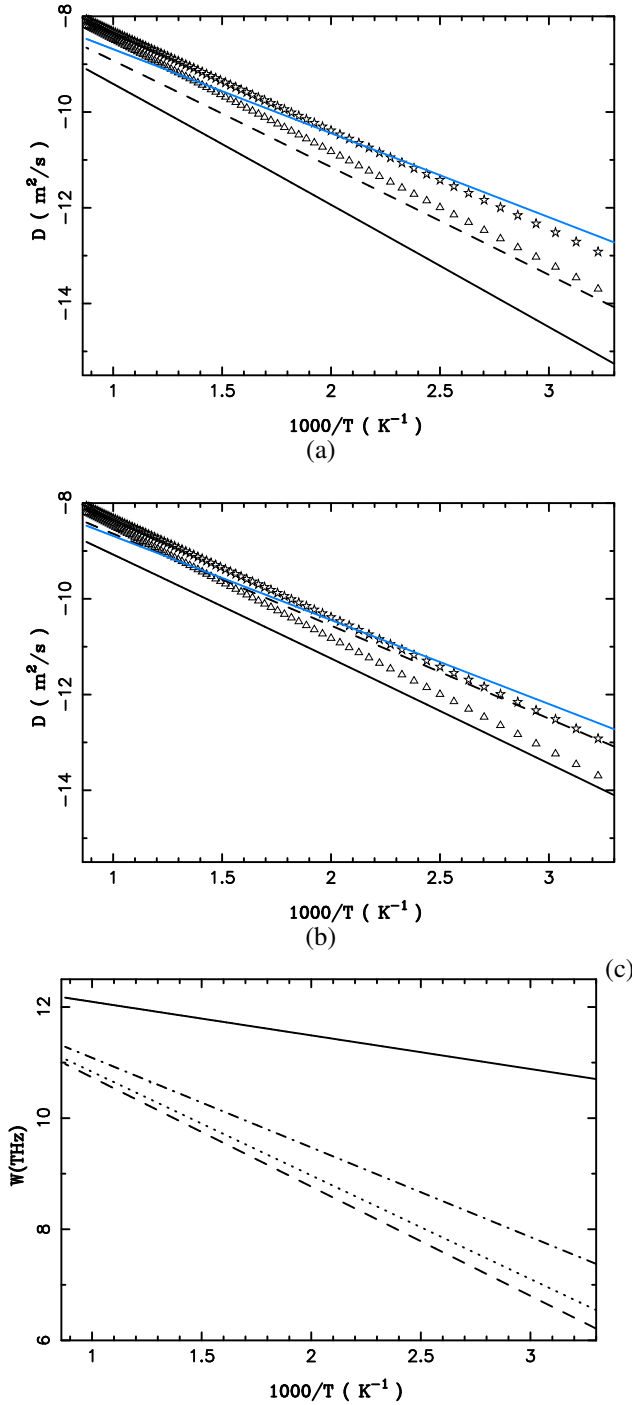


FIG. 3: Hydrogen diffusion coefficients vs $1/T$ (K^{-1}). The hydrogen diffusion coefficients D_c and D_a in black solid and dashed lines respectively, from present calculations with: (a) Siesta, and (b) Vasp. In open triangles and stars D_H from experimental data [36] and KMC results [35]. The experimental hydrogen diffusion coefficient in Zr-2.5Nb [38] (in blue solid line) is also shown. (c) Mean jump frequencies vs $1/T$ (K^{-1}). $\omega_1 > \omega_3 > \omega_4 > \omega_2$.

compared with experimental data in pure metal and the alloy Zr-2.5 Nb. Our results with Vasp reproduce very well the experimental data and the numerical results of KMC.

The anisotropy of the H diffusion in hcp Zr along the $\langle c \rangle$ and $\langle a \rangle$ axes, is measurable from the D_c/D_a ratio,

$$\frac{D_c}{D_a} = \frac{3c^2}{8a^2} \left(\frac{2\omega_{OO}}{3\omega_{OT}} + \frac{2\omega_{TT}}{2\omega_{TT} + 3\omega_{TO}} \right). \quad (12)$$

The dependence on the temperature of the ratio D_c/D_a , defined in Eq. (12) is through the mean jump frequencies ω_i . Fig. 4 shows that the results of the ratio D_c/D_a in Ref. [7] (symbols in orange) agree better with present results with Vasp (in dashed line) than with Siesta (solid line). Possibly because Siesta overestimate the values of the migration barriers.

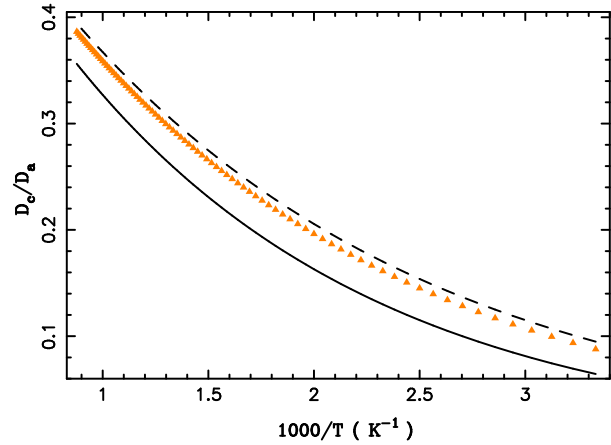


FIG. 4: D_c/D_a vs $1/T$ (in K^{-1}). Symbols in black show our results with Vasp (open stars) and Siesta (full stars). In orange the results in Ref. [7].

VI. ZIRCONIUM HYDRIDES

The three most stable zirconium-hydrides in Zr based alloys are δ , γ , ϵ . The δ hydride is the most frequent in Zr-2.5Nb which appears at slow speed of cooling low than $2^\circ\text{C}/\text{min}$. The composition of the δ -hydride is ZrH_x with $1.53 \leq x \leq 1.66$ (56.7 to 66% at Hydrogen, simulated as $\delta - \text{ZrH}_{1.5}$). This hydride forms plates located at the grain boundaries or trans-granular interphases.

This particular form is associated with the following relation of orientation: $(0002)_\alpha \parallel (111)_\delta$ and $[11\bar{2}0]_\alpha \parallel [110]_\delta$, which generates a $(10\bar{1}7)_\alpha$ plane that is practically parallel to the basal plane of Zr [39] and precipitates mostly in the radial direction, as shown in Fig. 5 [40].

We present our preliminary results in Table 5, of the three stable hydrides schematized in Fig. 6. Our results reproduce well the ones obtained by Glasoff [41]. We have followed the same methodology to familiarize ourselves with this type of structures. The equilibrium lattice constants were determined by lattice relaxation, minimizing the total energy of the system by varying atomic positions with the calculation parameters defined in Section II.

In Table 5, the values of the lattice parameter of each cell vary little from one hydride to another. Our results agree very well with the calculations made by Glasoff [41] and

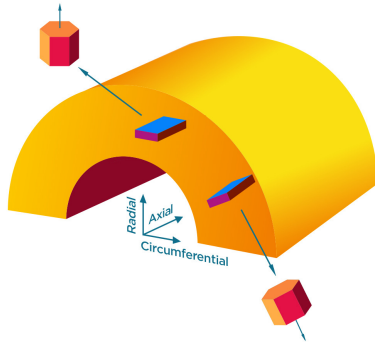


FIG. 5: Hydride's Radial and circumferential orientation in tubes of Zr-2.5Nb.

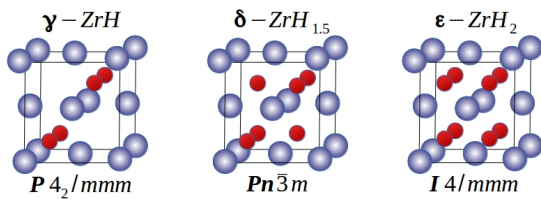


FIG. 6: Crystal structure of the 3 stable hydrides in zirconium: orthorhombic γ -ZrH; cubic δ -ZrH_{1.5} and tetragonal ϵ -ZrH₂.

with the available experimental data. The hydride formation enthalpy, E_f^x , is calculated as Glasoff [41].

TABLE 5: Lattice parameters (in Å) and the hydrogen solution energy (in eV) of the three stables hydrides in α Zr with Vasp.

System	γ -ZrH	δ -ZrH _{1.5}	ϵ -ZrH ₂
a	3.232	4.807	3.538
a [13]	3.223	4.482	3.537
a_{exp} [42]	3.243	4.777	3.520
c	5.016	4.807	4.406
c [13]	5.014	4.821	4.458
c_{exp} [42]	4.948	5.777	4.449
c/a	1.55	1.0	1.25
$c/a _{exp}$ [42]	1.53	1.0	1.26
E_f^x	-0.408	-0.564	-0.573
E_f^x [13]	-0.32	-0.548	-0.556

VII. CONCLUSIONS

In summary, we have studied the hydrogen diffusion by ab initio methods in α Zr. Also, the energetic of hydrogen in the Zr-Nb system were also studied. We remark that,

- our DFT results of the lattice parameters are in well agreement with the experimental values.
- The calculated formation energies are within the range of values of previous references and experimental values.
- The mixing energy in the dilute limit shows that Zr is energetically favorable to dissolve in the bcc phase of

Nb, and on the contrary, Nb has a low solubility in hcp Zr.

- The presence of Nb in hcp Zr moderately increases the solubility of H around the impurity, implying in a slight reduction in diffusivity of the H by trapping H locally, forming the H-Nb complex.
- The hydrogen solution energy shows that tetrahedral sites are the most stable for H.
- The H-diffusion coefficient in hcp Zr, calculated with Vasp reproduce very well the experimental values and previous results from KMC.

ACKNOWLEDGEMENTS

We want to thank Dr. Gladys Domizzi for her comments on the manuscript. This work was partially financed by CONICET PIP-11220170100021CO.

REFERENCIAS

- [1] G. Beltramo, V. Ramunni y R. Pasianot. Theoretical and numerical study of hydrogen diffusion in Zr-Nb alloys. *Anales AFA* **32**, 112-119 (2021).
- [2] V. P. Ramunni, M. A. Alurralde y R. C. Pasianot. Search of point defect transition states in hcp twin boundaries: The monomer method. *Phys. Rev. B* **74**, 054113 (2006).
- [3] G. Henkelman y H. Jónsson. A dimer method for finding saddle points on high dimensional potential surfaces using only first derivatives. *J. Chem. Phys.* **111**, 7010-7022 (1999).
- [4] G. Kresse y J. Hafner. Ab initio molecular-dynamics simulation of the liquid-metal-amorphous-semiconductor transition in germanium. *Phys. Rev. B* **49**, 14251-14269 (1994).
- [5] J. M. Soler, E. Artacho, J. D. Gale, A. García, J. Junquera, P. Ordejón y D. Sánchez-Portal. The SIESTA method for ab initio order-N materials simulation. *J. Phys. Condens. Matter* **14**, 2745-2779 (2002).
- [6] R. Pasianot, R. Pérez, V. Ramunni y M. Weissmann. Ab initio approach to the effect of Fe on the diffusion in hcp Zr II: The energy barriers. *J. Nucl. Mater.* **392**, 100-104 (2009).
- [7] Y. Zhang, C. Jiang y X. Bai. Anisotropic hydrogen diffusion in α -Zr and Zircaloy predicted by accelerated kinetic Monte Carlo simulations. *Sci. Rep.* **7**, 41033 (2017).
- [8] F. Birch. Finite Elastic Strain of Cubic Crystals. *Phys. Rev.* **71**, 809-824 (1947).
- [9] J. P. Perdew, K. Burke y M. Ernzerhof. Generalized Gradient Approximation Made Simple. *Phys. Rev. Lett.* **77**, 3865-3868 (1996).
- [10] P. E. Blöchl, O. Jepsen y O. K. Andersen. Improved tetrahedron method for Brillouin-zone integrations. *Phys. Rev. B* **49**, 16223-16233 (1994).
- [11] H. J. Monkhorst y J. D. Pack. Special points for Brillouin-zone integrations. *Phys. Rev. B* **13**, 5188-5192 (1976).
- [12] R. Pasianot y A. Monti. A many body potential for α -Zr. Application to defect properties. *J. Nucl. Mater.* **264**, 198-205 (1999).

- [13] M. Christensen, W. Wolf, C. Freeman, E. Wimmer, R. B. Adamson, L. Hallstadius, P. E. Cantonwine y E. V. Mader. H in α -Zr and in zirconium hydrides: solubility, effect on dimensional changes, and the role of defects. *J. Phys. Condens. Matter* **27**, 025402 (2015).
- [14] D. R. Lide. *CRC handbook of chemistry and physics: a ready-reference book of chemical and physical data* (CRC press, Boca Raton, Florida, 1995).
- [15] J. Goldak, L. T. Lloyd y C. S. Barrett. Lattice Parameters, Thermal Expansions, and Grüneisen Coefficients of Zirconium, 4.2 to 1130°K. *Phys. Rev.* **144**, 478-484 (1966).
- [16] C. Kittel. *Introduction to Solid State Physics* (Wiley, New York, 2005).
- [17] H. H. Neely. Damage rate and recovery measurements on zirconium after electron irradiation at low temperatures. *Radiation Effects* **3**, 189-201 (1970).
- [18] G. Hood y R. Schultz. Defect recovery in electron-irradiated α -Zr single crystals: A positron annihilation study. *J. Nucl. Mater.* **151**, 172-180 (1988).
- [19] M. Cottura y E. Clouet. Solubility in Zr-Nb alloys from first-principles. *Acta Mater.* **144**, 21-30 (2018).
- [20] D.-Y. Lin, S. S. Wang, D. L. Peng, M. Li y X. D. Hui. Ann-body potential for a Zr-Nb system based on the embedded-atom method. *J. Phys. Condens. Matter* **25**, 105404 (2013).
- [21] R. Roberge. Lattice parameter of niobium between 4.2 and 300 K. *Journal of the Less Common Metals* **40**, 161-164 (1975).
- [22] P. Söderlind, L. H. Yang, J. A. Moriarty y J. M. Wills. First-principles formation energies of monovacancies in bcc transition metals. *Phys. Rev. B* **61**, 2579-2586 (2000).
- [23] M. I. Baskes. Modified embedded-atom potentials for cubic materials and impurities. *Phys. Rev. B* **46**, 2727-2742 (1992).
- [24] H. Ullmaier, P. Ehrhart, P. Jung y H. Schultz. *Atomic defects in metals* (Springer, Berlin, 1991).
- [25] V. O. Kharchenko y D. O. Kharchenko. Ab-initio calculations for the structural properties of Zr-Nb alloys. *Condens. Matter Phys.* **16**, 13801 (2013).
- [26] C. Domain. Ab initio modelling of defect properties with substitutional and interstitial elements in steels and Zr alloys. *J. Nucl. Mater.* **351**, 1-19 (2006).
- [27] X. Xin, W. Lai y B. Liu. Point defect properties in hcp and bcc Zr with trace solute Nb revealed by ab initio calculations. *J. Nucl. Mater.* **393**, 197-202 (2009).
- [28] D. Jiang y E. A. Carter. First principles assessment of ideal fracture energies of materials with mobile impurities: implications for hydrogen embrittlement of metals. *Acta Mater.* **52**, 4801-4807 (2004).
- [29] K. Huber y G. Herzberg. *Molecular Spectra and Molecular Structure IV. Constants of Diatomic Molecules* (Van Nostrand Reinhold Co, 1979).
- [30] C. Varvenne, O. Mackain, L. Proville y E. Clouet. Hydrogen and vacancy clustering in zirconium. *Acta Mater.* **102**, 56-69 (2016).
- [31] K. Lee, M. Yuan y J. Wilcox. Understanding Deviations in Hydrogen Solubility Predictions in Transition Metals through First-Principles Calculations. *J. Phys. Chem. C* **119**, 19642-19653 (2015).
- [32] C. Domain, R. Besson y A. Legris. Atomic-scale Ab-initio study of the Zr-H system: I. Bulk properties. *Acta Mater.* **50**, 3513-3526 (2002).
- [33] S. Ishioka y M. Koiwa. Diffusion coefficient in crystals with multiple jump frequencies. *Philos. Mag. A* **52**, 267-277 (1985).
- [34] G. H. Vineyard. Frequency factors and isotope effects in solid state rate processes. *J. Phys. Chem. Solids* **3**, 121-127 (1957).
- [35] A. Sawatzky, A. Ledoux, R. Tough y C. Cann. *Miami International Symposium: April 1981* 109-120 (Oxford: Pergamon Press, Miami Beach, Florida, 1982).
- [36] J. Kearns. Diffusion coefficient of hydrogen in alpha zirconium, Zircaloy-2 and Zircaloy-4. *J. Nucl. Mater.* **43**, 330-338 (1972).
- [37] C.-S. Zhang, B. Li y P. Norton. The study of hydrogen segregation on Zr(0001) and Zr(1010) surfaces by static secondary ion mass spectroscopy, work function, Auger electron spectroscopy and nuclear reaction analysis. *J. Alloys Compd.* **231**, 354-363 (1995).
- [38] G. McRae, C. Coleman, H. Nordin, B. Leitch y S. Hanlon. Diffusivity of hydrogen isotopes in the alpha phase of zirconium alloys interpreted with the Einstein flux equation. *J. Nucl. Mater.* **510**, 337-347 (2018).
- [39] D. Northwood y R. Gilbert. Hydrides in zirconium-2.5 wt.% niobium alloy pressure tubing. *J. Nucl. Mater.* **78**, 112-116 (1978).
- [40] M. Leger, G. Moan, A. Wallace y N. Watson. *Zirconium in the Nuclear Industry: 8 th Int. Symposium* (ASTM STP 1023, Philadelphia, 1979).
- [41] M. V. Glazoff. *Modeling of Some Physical Properties of Zirconium Alloys for Nuclear Applications in Support of UFD Campaign* inf. téc. (2013).
- [42] S. S. Sidhu, N. S. S. Murthy, F. P. Campos y D. D. Zaubers. en *Advances in Chemistry* 87-98 (1963).